AIAA JOURNAL
Vol. 42, No. 12, December 2004

Breakup of Round Nonturbulent Liquid Jets in Gaseous Crossflow

K. A. Sallam*
Oklahoma State University, Stillwater, Oklahoma 74078
and
C. Aalburg† and G. M. Faeth‡
University of Michigan, Ann Arbor, Michigan 48109

An experimental investigation of the primary breakup of round nonturbulent liquid jets in gaseous crossflow is described. Pulsed shadowgraph and holograph observations were made to determine the following breakup properties: primary breakup regimes, conditions required for the onset of ligament and drop formation, ligament and drop sizes along the liquid surface, drop velocities after breakup, rates of liquid breakup along the liquid surface, conditions required for the breakup of the liquid column as a whole, and liquid column trajectories. These observations were made for round nonturbulent liquid jets in subsonic crossflow at normal temperature and pressure. The results suggest qualitative similarities between the primary breakup of nonturbulent round liquid jets in gaseous crossflow and the secondary breakup of drops subjected to shock wave disturbances. Phenomenological analyses were effective to help interpret and correlate the new measurements of the primary breakup properties of nonturbulent round liquid jets in gaseous crossflow.

Nomenclature

C_D = drag coefficient
C_ℓ = empirical constant for the shear layer thickness; Eq. (15)
$C_{\ell i}$ = empirical constant for the onset of ligament formation; Eq. (4)
C_{pi} = empirical constant for the onset of drop formation; Eq. (5)
C_t = empirical constant for the time of onset of ligament formation; Eq. (11)
C_{xb} = empirical constant for the cross stream penetration of the liquid column; Eq. (23)
C_{yb} = empirical constant for the time of breakup of the liquid column; Eq. (21)
d_i = streamwise jet diameter at onset of drop formation
d_{inj} = injector passage diameter
d_j = liquid jet diameter at jet exit
d_ℓ = diameter of ligaments along the liquid jet surface
d_p = diameter of drops formed by primary breakup
L = injector passage length
L_b = liquid jet breakup length
Oh = liquid jet Ohnesorge number, $\mu_L/(\rho_L d_j \sigma)^{1/2}$
q = jet momentum ratio, $\rho_L v_j^2/(\rho_G u_\infty^2)$
Re = liquid jet Reynolds number, $v_j d_j/\nu_L$
t = time
t^* = characteristic time, $d_j(\rho_L/\rho_G)^{1/2}/u_\infty$
t_v^* = characteristic viscous time, d_j^2/ν_L
u = cross stream velocity
v = streamwise velocity
We = crossflow Weber number, $\rho_G d_j u_\infty^2/\sigma$
x = cross stream distance
y = streamwise distance
δ = shear layer thickness
ε = surface efficiency factor; Eq. (27)
λ_s = wavelength of liquid surface waves
μ = molecular viscosity
ν = kinematic viscosity
ρ = density
σ = surface tension

Subscripts

b = location of breakup of entire liquid jet
G = gas property
i = location of onset of breakup
j = jet exit property
L = liquid property
ℓ = ligament property
p = property of drops formed by primary breakup
∞ = ambient gas property

Received 10 July 2003; revision received 23 July 2004; accepted for publication 5 August 2004.

*Assistant Professor, School of Mechanical and Aerospace Engineering.
†Research Fellow, Department of Aerospace Engineering.
‡A. B. Modine Distinguished University Professor, Department of Aerospace Engineering. Fellow AIAA.

Introduction

THE deformation and primary breakup properties of round nonturbulent liquid jets in gaseous crossflow were studied experimentally, motivated by applications to spray breakup in crossflow in airbreathing propulsion systems, liquid rocket engines, diesel engines, and agricultural sprays, among others. The objective was to extend recent shadowgraphy measurements of Mazallon et al.[1] and Wu et al.[2] of some properties of this liquid breakup process to exploit the capabilities of pulsed holography to penetrate dense sprays and observe the detailed properties of both the liquid surface and the primary breakup process at the liquid surface.

Earlier studies of the primary breakup of round nonturbulent liquid jets in gaseous crossflow were recently reviewed by Wu et al.[2]; therefore, the following discussion of past work will be brief. Initial studies of round nonturbulent liquid jets in gaseous crossflow mainly concentrated on lengths of penetration of the liquid jet into the crossflow and the trajectories of the liquid column for various flow conditions.[3–14] Additional details about the properties of round nonturbulent liquid jets in gaseous crossflow were recently obtained by Mazallon et al.[1] and Wu et al.,[2] and references cited therein, using pulsed shadowgraphy. These studies reported similarities between the primary breakup regimes of round nonturbulent liquid jets in gaseous crossflow and the secondary breakup of drops due to shock wave disturbances. In particular, both studies observed bag, multimode, and shear breakup regimes along the liquid column in crossflow that were qualitatively similar to secondary drop breakup regimes having the same names. Other properties of

round nonturbulent liquid column breakup in gaseous crossflow that were observed using pulsed shadowgraphy during these studies were as follows: wavelengths of liquid surface waves along the liquid column, the deformation of the liquid column before the onset of breakup along the liquid surface, the conditions for the onset of drop formation along the liquid surface, and the trajectory of the liquid column as it deflects due to crossflow.

The objectives of the present investigation were to extend the studies of Mazallon et al.[1] and Wu et al.,[2] using the capabilities pulsed holography to penetrate the dense spray region and observe the liquid breakup process near the surface of the liquid jet. Observations of Mazallon et al.[1] and Wu et al.[2] of conditions for breakup regime transitions, of wavelengths of liquid surface waves along the liquid surface, of the deformation of the liquid column before the onset of breakup along the liquid surface, and of the trajectory of the liquid column as it deflects in the crossflow were revisited. In addition, breakup properties at the liquid surface were also observed, as follows: the properties of the liquid surface (surface velocities, the onset of ligament formation, and ligament properties), the properties of liquid drops formed by primary breakup along the liquid surface (the onset of drop formation, drop sizes and velocities after primary breakup, and rates of drop formation along the liquid surface), and conditions required for the breakup of the liquid jet as a whole (ending the primary breakup process). Finally, phenomenological analyses were used to help interpret the results and correlate the measurements for use by others.

Experimental Methods

Apparatus

Observations of liquid breakup along the surface of the liquid jet were carried out using a shock tube apparatus, whereas measurements of the length of the liquid column in the liquid column breakup regime were carried out using a subsonic wind tunnel. The shock tube had a rectangular cross section with a width of 38 mm and a height of 64 mm. The driven section of the shock tube was open to the atmosphere and had windowed side walls to provide optical access. The shock tube was sized to provide test times of 17–21 ms in the uniform subsonic flow region behind the shock wave. Crossflow velocities in air of 11–142 m/s were considered for normal temperature and pressure conditions in the crossflow.

The shock tube apparatus did not provide a large enough cross section to observe breakup of the entire liquid column in the liquid column breakup regime for crossflow at normal temperature and pressure conditions; therefore, observation of these properties were carried out in a subsonic wind tunnel having a cross section of 610×610 mm. The wind tunnel had windowed side walls to provide optical access with air crossflow having velocities of 5–15 m/s at normal temperature and pressure.

The nonturbulent round liquid jets were injected vertically downward using a pressure feed system for both the shock tube and wind-tunnel arrangements. The test liquid was contained within a cylindrical liquid supply chamber having a diameter of 50 mm and a length of 100 mm, constructed of type 304 stainless steel. The injector passage was located along the bottom of the liquid supply chamber and was directed along the chamber axis. Round supercavitating nozzles were used to create the round nonturbulent liquid jets; these nozzles had sharp-edged inlets and exits with length-to-diameter ratios smaller than 3. This arrangement yielded uniform nonturbulent round liquid jets as discussed by Wu et al.[15] and Lienhard.[16] Supercavitating nozzles having diameters of 0.5, 1.0, and 2.0 mm were used. These supercavitating nozzles were manufactured by drilling each of these hole sizes into a 3-mm-thick stainless-steel plate and counterboring the plate with a 90-deg included angle cone leaving a constant diameter section less than 0.3 mm long. With this configuration, reattachment of the jets in the short constant area section did not occur, which was evident from shadowgraphs showing that the liquid jets had smooth surfaces in the absence of crossflow. Actual liquid diameters at the jet exit were found from shadowgraphs with an experimental uncertainty (95% confidence) less than 10%; these diameters were only 50–70% of the geometrical nozzle exit diameters as discussed by Lienhard.[16]

The test liquid was placed in the liquid supply chamber using a fill line. During the filling process, surface tension at the jet exit was sufficient to prevent premature outflow of the test liquid. Pressurized air was admitted to the top of the test chamber on activation of a solenoid valve to initiate the flow of the liquid jet. The air used to pressurize the jet liquid was stored in an air reservoir having a volume of 1.3 m^3. The air reservoir was set to the desired injection pressure by filling from the laboratory air supply system. (The air supply pressures were up to 1.5 MPa, and the air dewpoints were smaller than 240 K.) The increased pressure in the liquid supply chamber then caused liquid outflow through the nozzle. Significant aeration of the test liquid was prevented in several ways: A baffle was placed across the air inlet of the liquid supply chamber to prevent high-velocity gas from contacting the liquid surface, the cross-sectional area of the liquid supply chamber was large compared to the nozzle cross-sectional area so that streamwise gas velocities at the liquid surface were small (less than 70 mm/s), and liquid during present observations was drawn from the bottom of the liquid supply chamber well away from the liquid surface where there was potential for aeration of the liquid. These measures to prevent aeration of the liquid surface were effective, based on observations of the liquid jet in the absence of crossflow where the surface was smooth allowing observations of the bulk liquid that did not reveal the presence of any bubbles. Once all of the liquid was forced out of the liquid supply chamber, the solenoid valve was closed and the liquid supply chamber was then refilled for the next test.

Test times were short for the shock tube arrangement, less than 20 ms; however, this was not a problem because flow development times (the time required for a given liquid sample to cross the flow cross section) were smaller than one-third of the available test times. In addition, data acquisition times, using pulsed shadowgraphy and holography, were even shorter, less than 10 ns, and did not impose any significant test time requirements. Operation was essentially steady for the wind-tunnel apparatus, and flow development did not pose any limitations of these measurements as well.

The potential uniformity of the crossflow acting on the round nonturbulent liquid jets is an important issue, as discussed by Mazallon et al.[1] For the present shock tube experiments, measurements were obtained at relatively short residence times (less than 20 ms) after the passage of a propagating shock wave past the liquid jet location. This implies that the characteristic thickness of the nonuniform velocity field in the boundary layer along the shock tube walls was generally less than 0.5 mm, based on the transient analysis presented by Schlichting.[17] This disturbed region was smaller than 10% of the distance along the liquid jet for all observation conditions considered during the shock tube experiments of the present investigation so that the disturbance of the flow due to the presence of the wall boundary layer was not significant within present experimental uncertainties. Finally, the wind-tunnel apparatus was limited to consideration of liquid column breakup, which only occurs at rather large distances from the jet exit; therefore, the effect of the wall boundary layer for these experiments was generally even smaller than for the shock tube experiments.

Instrumentation

Pulsed shadowgraphy and holography were used for the shock tube experiments to observe the properties of the round liquid jets and the ligaments and drops produced by primary breakup as a function of position along the liquid jet and crossflow conditions. The arrangement of the shadowgraphy and holography systems was similar to earlier work using these instruments to study the secondary breakup of drops.[18–23] Both measurements used two frequency-doubled YAG lasers (Spectra Physics Model GCR-130, 532-nm wavelength, 7-ns pulse duration, and up to 300-mJ optical energy per pulse) that could be fired with pulse separations as small as 100 ns. An off-axis holocamera arrangement was used that provided a 25 mm diameter field of view at the test liquid column location. Reconstruction of the double-pulse holograms yielded two images of the flow so that liquid surface and drop velocities could be found given the time of separation of the laser pulses (which was measured using a digital oscilloscope). The second laser pulse was weaker than

the first, which allowed directional ambiguity to be resolved because stronger laser pulses yielded sharper reconstructed images. The same arrangement provided shadowgraph images simply by blocking the reference beam.

The hologram reconstruction system used to analyze the hologram and shadowgraph images from the shock tube involved a helium–neon laser (Spectra Physics Model 124B, continuous wave laser, 35 mW of optical power). The reconstructed image was observed using a charge-coupled device camera (Sony, Model XC-77) having optics to yield a magnification of 300:1 and a field of view of the image on the monitor of 1.2×1.4 mm. The optical data was obtained using a frame grabber (Data Translation DT2851) and processed using Media Cybernetics Image-Pro Plus software. Various locations in the hologram reconstruction were observed by traversing the hologram parallel to the crossflow and the jet directions and traversing the video camera of the image display system in the direction normal to this plane. Positions were selected for viewing using stepping-motor-driven linear traversing systems (Velmex, Model VP9000) having 1000-nm positioning accuracies. The combined holocamera/reconstruction system allowed objects as small as 3000 nm to be seen and the size of objects as small as 10,000 nm to be measured with 10% accuracy. The reconstruction system was also used to measure flow properties from shadowgraph photographs with the photographs placed in the hologram holder, which allowed two-dimensional traversing as before.

Drop sizes and velocities were measured as described by Hsiang and Faeth[18–20] and Chou et al.,[21] whereas ligament and liquid surface properties were found similar to Sallam et al.[24] Drops generally were spherical and could be represented by an average diameter; ligaments were roughly cylindrical and could also be represented by an average diameter. Experimental uncertainties (95% confidence) were found using standard methods similar to past work.[18–21] These uncertainties were less than 10%, for drop diameters larger than 10,000 nm, increasing inversely proportional to the drop diameter for smaller sized drops. Drop velocities were found from simple arithmetic averages (because drop velocity distributions were nearly uniform) with experimental uncertainties (95% confidence) less than 10%. In all cases, the numbers of drops or ligaments measured at a point was selected to achieve the experimental uncertainties just mentioned.

Liquid column properties observed using the wind-tunnel facility were obtained from single-pulse shadowgraphs. Streamwise and cross stream distances between the end of the liquid column and the jet exit were obtained from these shadowgraphs with experimental uncertainties (95% confidence) smaller than 10%.

Test Conditions

Test conditions are summarized in Table 1. Liquid properties in Table 1 were measured as follows: liquid densities using a set of precision hygrometers (Fisher Model 11-582; 0.1% accuracy), liquid viscosity using a Cannon–Fenske viscometer (Fisher Model 13-617; 3% accuracy), and surface tension using a ring tensiometer (Fisher Model 20; 1% accuracy). The present results for pure fluids agreed with values of Lange,[25] within the accuracy of the instruments.

Test conditions were varied by considering four different liquids [water, ethyl alcohol, and glycerol (79 and 84% glycerin by mass)]; injector passage diameters of 0.5, 1.0, and 2.0 mm; liquid jet velocities of 7–45 m/s; and air crossflow velocities of 6–142 m/s at normal temperature and pressure. This yielded the following ranges of test variables: liquid/gas density ratios of 683–1033, actual liquid jet exit diameters d_j of 0.34–1.7 mm, liquid jet Reynolds numbers Re of 5×10^2–5.9×10^4, crossflow Weber numbers of 0.5–260, liquid/gas momentum flux ratios q of 3–450, and liquid jet Ohnesorge numbers Oh of 0.003–0.29. (See the Nomenclature for present definitions of these variables.) Crossflow Mach numbers were smaller than 0.1; therefore, compressibility effects were negligible.

Results and Discussion

Flow Visualization

The appearance of the various primary breakup processes that were observed for round nonturbulent liquid jets in gaseous crossflow is illustrated by the pulsed shadowgraph photographs appearing in Fig. 1. These test conditions involved water jets from an injector having an exit diameter of 1 mm, yielding an initial liquid jet diameter of 0.8 mm, for gaseous crossflow represented by the crossflow Weber number. These results, however, are typical of present results at other test conditions as well as the earlier observations of Mazallon et al.[1] Figure 1a, showing the liquid jet, for $We = 0$, exhibits a smooth liquid surface with no disturbances or protrusions of the surface of the liquid column and no initiation of atomization, even though the jet Reynolds number at this condition is relatively large, $Re = 3 \times 10^4$. This behavior is similar to past observations of atomization using round supercavitating injectors having a similar design that produce nonturbulent liquid jets; see Wu et al.[15] and Lienhard.[16] All liquid jet operating conditions considered during the present investigation had similar smooth liquid surfaces with no significant deformation, variation of jet cross stream diameter, or initiation of atomization, over the length of the jet when there was no crossflow. These results provide direct evidence that the primary breakup processes observed during the present investigation were caused by air crossflow rather than by liquid vorticity or turbulence, which is responsible for other liquid jet breakup processes, such as turbulent primary breakup considered by Sallam et al.[24] As a result, present measurements of breakup properties are defined by the crossflow Weber number We and are essentially independent of the streamwise liquid jet velocity as characterized by the momentum ratio q for the present range of this variable.

For present conditions, where effects of liquid viscosity were small ($Oh \leq 0.3$), four regimes of primary breakup of the liquid jets were observed for fixed liquid jet exit conditions as the crossflow velocity (characterized by the crossflow Weber number We) was increased, as follows: column breakup, bag breakup, multimode (or

Table 1 Summary of test conditions[a]

Liquid	Water	Ethyl alcohol	Glycerol 79%[b]	Glycerol 84%[b]
Density, kg/m^3	997	806	1205	1219
Liquid/gas density ratio ρ_L/ρ_G	845	683	1021	1033
Liquid viscosity, kg/m · s $\times 10^4$	8.94	12.3	323	804
Liquid/gas viscosity ratio μ_L/μ_G	48	66	2016	4346
Surface tension, N/m $\times 10^3$	70.8	24.0	59.8	63.0
Injector exit passage diameter, mm	0.5, 1.0, 2.0	1.0, 2.0	1.0, 2.0	1.0
Liquid jet exit diameter, mm[c]	0.34, 0.80, 1.6	0.9, 1.6	0.9, 1.7	0.9
Liquid jet Reynolds number Re	(3.8–59) $\times 10^3$	(8–32) $\times 10^3$	(5–40) $\times 10^2$	(1.6–3.7) $\times 10^3$
Liquid jet Weber number We	0.5–260	2–260	3–260	3–250
Liquid/gas momentum ratio q	3–200	20–100	70–100	65–450
Liquid jet Ohnesorge number $Oh \times 10^3$	3–5	80–120	140	290

[a]Air crossflow at 98.8 kPa and 298 K; properties of air were found at normal temperature and pressure: $\rho_G = 1.18$ kg/m^3 and $\mu_G = 18.5 \times 10^{-6}$ kg/m · s.
[b]Percentage of glycerin by mass.
[c]Actual diameter of the nonturbulent liquid jet after contraction following passage through the supercritical nozzle.

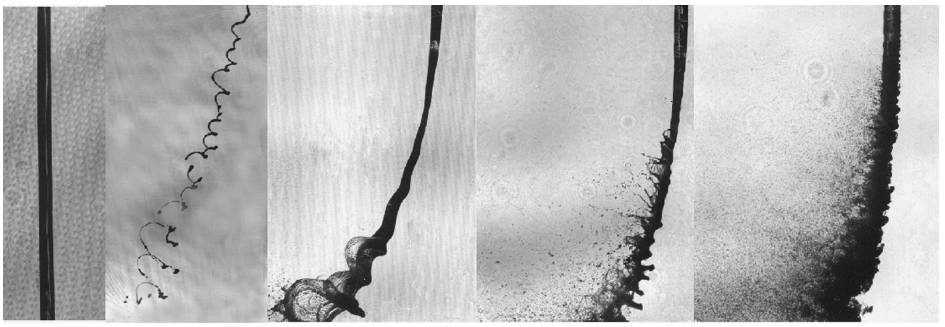

Fig. 1 Visualization of primary breakup processes of round nonturbulent liquid jets in gaseous crossflow: a) *We* = 0, no breakup; b) *We* = 3, column breakup; c) *We* = 8, bag breakup; d) *We* = 30, multimode breakup; and e) *We* = 220, shear breakup.

bag/shear) breakup, and shear breakup, as shown in Figs. 1b–1e. At the smallest velocities, $We \leq 4$, the liquid jet column was somewhat deformed, to yield an ellipsoidal cross section, and deflected in the direction of the crossflow velocity. This behavior is caused by reduced gas pressures along the sides of the jet due to acceleration of the gas across the liquid jet, with the lateral motion of the liquid jet eventually stabilized by surface tension. This behavior is somewhat analogous to the behavior of individual drops during secondary breakup when subjected to shock wave disturbances in the deformation regime.[18–23] The increased drag forces due to the flattened shape of the liquid jet enhances its tendency to be deflected in the crossflow direction due to the gaseous crossflow. Given some degree of flattening of the liquid jet, somewhat thicker nodelike regions begin to appear along the length of the liquid jet with distances between the nodes generally comprising several liquid jet diameters. The spacing of these nodes progressively decreases with increasing crossflow Weber numbers. Subsequently, larger accelerations of the cylindrical liquid connections between the nodes cause them to be deflected in the crossflow direction more rapidly than the nodes, giving the liquid jet a looplike structure. Finally, continued deflection of the connections in the crossflow direction relative to the nodes eventually causes the connections to break, with the resulting free sections of the liquid connections eventually forming a string of drops along their length by a process very similar to Rayleigh breakup of liquid jets, leaving the nodes as larger drops among the rest. The general appearance of the flow at these conditions can be seen at the bottom of Fig. 1b.

As crossflow velocities increase, the next primary breakup regime that is observed for $We = 4$–30, is the bag breakup regime. Bag breakup appears in Fig. 1c, for $We = 8$. In this regime, crossflow Weber numbers have reached values where the spacing between the nodes is comparable to the liquid jet diameter. Once the liquid jet has flattened significantly between the nodes, baglike structures appear between the nodes that are very similar to the baglike structures appearing at the center of the deformed drops in the bag breakup regime observed during the secondary breakup of drops subjected to shock wave disturbances.[18–20] This behavior involves the formation of bags as a result of the deformation of the central portion of the liquid jet between nodes due to the higher pressure of the stagnating gas flow on the upstream side of the liquid jet than on its downstream side. With increasing distance along the liquid column (or time in the crossflow), the bags grow in the crossflow direction and then begin to progressively break up, beginning at their farthest position of deflection in the crossflow direction (or tip), in a mechanism very similar to the bag breakup of drops undergoing secondary breakup due to shock wave disturbances.[22] This is followed by breakup of the connecting liquid columns between the nodes, and along the sides of the bags, into relatively large drops, once again by the mechanism of Rayleigh breakup, similar to bag breakup during secondary drop breakup due to shock wave disturbances.[22] This behavior tends to separate drops according to size along the liquid column, with the smallest drops formed by breakup of the bag appearing first, followed by larger drops formed by breakup of the connecting liquid columns, and finally the largest drops that are associated with the nodes.

Shifting to conditions at the largest crossflow velocities considered during the present investigation (or the largest crossflow Weber numbers), $We > 110$, primary jet breakup enters the shear breakup regime. Shear breakup appears in Fig. 1e, for $We = 220$. Similar to column and bag breakup, the shear breakup process begins by deflection of the liquid jet in the crossflow direction, but with negligible distortion of the jet cross section. In this case, wavelike disturbances appear on the upstream side of the deflected liquid jet, probably as a result of Rayleigh/Taylor instabilities, that is, as a result of acceleration of a fluid of greater density toward a fluid of lesser density in this region. The spacing of these disturbances along the liquid jet is on the order of 0.1 of the jet diameter, and they do not develop into the nodes observed in the liquid column and bag breakup regimes. Instead, they grow into ligaments that form along the periphery of the liquid jet and separate from its downstream side (in the crossflow direction). These ligaments are terminated when drops form from their ends, very similar to secondary drop breakup when drops are subjected to shock wave disturbances in the shear breakup regime.[18–21] With increasing distance along the liquid jet, the distance between these disturbances tends to increase, resulting in progressively increasing diameters of both the ligaments and of the drops forming from the end of the ligaments. This behavior is also analogous to the progressive increase of the size of the ligaments, and the drops formed from them, as a function of time, during secondary drop breakup when drops are subjected to shock wave disturbances in the shear breakup regime.[18–21]

Finally, there is a range of crossflow velocities, for $We = 30$–110, between the bag and shear breakup regimes, that involves a complex mixture of the properties of the bag and shear breakup regimes, called the multimode (or bag/shear) breakup regime.[1] Multimode breakup, for $We = 30$, is shown in Fig. 1d. In this case, the spacing between disturbances along the surface of the jet is such that formation of both bags and ligaments can be accommodated, leading to a regime of breakup of round liquid jets in crossflow analogous to the multimode breakup regime for the secondary breakup of drops subjected to shock wave disturbances.

Primary Breakup Regimes

By the exploitation of the similarities between the primary breakup regimes of round nonturbulent liquid jets in crossflow, and the secondary breakup of drops subjected to shock wave disturbances, the breakup regimes of round nonturbulent liquid jets in crossflow were correlated in terms of crossflow Weber and Ohnesorge numbers as first proposed by Hinze[26] for the secondary breakup of drops exposed to shock wave disturbances at large liquid/gas density ratio conditions similar to present observations. This approach has also been used subsequently by most investigators of secondary drop breakup; see Refs. 18–23 and references cited therein. It is easily shown that the crossflow Weber and Ohnesorge numbers govern breakup regime transitions: For conditions where viscous forces are small, gasdynamic forces (or drag) on the liquid jet must be stabilized by surface tension forces, which implies that deformation and breakup regime transitions correspond to particular critical Weber numbers, that is, $We_{cr} = \text{const}$, whereas,

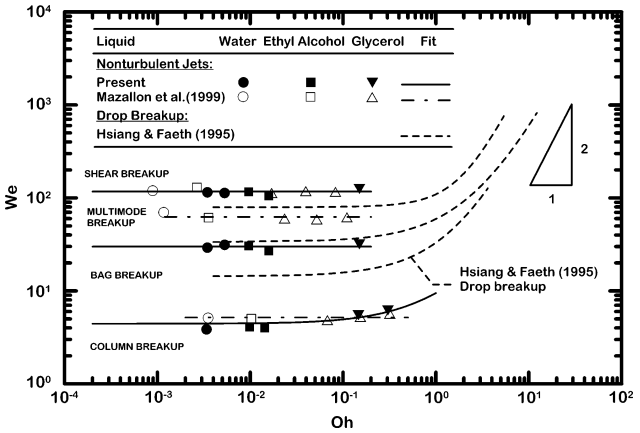

Fig. 2 Primary breakup regime map for nonturbulent round liquid jets in gaseous crossflow.

for conditions where surface tension forces are small, gasdynamic forces (drag) on the liquid jet must be stabilized by liquid viscous forces, which implies that critical crossflow Weber numbers are proportional to the square of the Ohnesorge number, that is, $We_{cr} \sim Oh^2$; see Hsiang and Faeth.[20]

The primary breakup regime map for liquid jets in gaseous crossflows is plotted in terms of the Hinze[26] coordinates in Fig. 2, with the symbols denoting conditions where roughly half of the observations corresponded to conditions within the two bounding regimes, similar to past work for the primary breakup of liquid jets in gaseous crossflow due to Mazallon et al.[1] and the secondary breakup of drops due to shock wave disturbances due to Hsiang and Faeth.[20] Experimental uncertainties (95% confidence) of these boundaries are smaller than 25% for Weber number We and 5% for Ohnesorge number Oh (which has a small effect for the test range of liquid jets in Fig. 2 in any event). Also shown in Fig. 2 are earlier determinations of the breakup regime boundaries of nonturbulent round liquid jets in crossflow from Mazallon et al.[1] and for the secondary breakup of drops subjected to shock wave disturbances from Hsiang and Faeth.[20]

The breakup regime boundaries for liquid jets in crossflow from Mazallon et al.[1] and the present investigation are qualitatively similar. The value of $Oh < 0.3$ for these experimental conditions. Liquid viscous effects are small at these conditions, which implies constant values of the Weber number We at the various transitions as observed for the results shown in Fig. 2, as discussed earlier. The effects of the liquid-jet/crossflow momentum ratio, $q = \rho_L v_j^2/(\rho_G u_\infty^2)$, on breakup regime transitions were negligible for present test conditions, which involve $q = 3$–450. This behavior agrees with the earlier findings of Mazallon et al.[1] over the range of $q = 100$–8000. This effect seems quite reasonable, however, in view of the inability of even large jet exit velocities to cause breakup in the absence of a crossflow, as shown in Fig. 1a. In general, increasing liquid jet velocities simply stretched out the breakup process in the liquid jet streamwise y direction, with little other effect except for modifying drop velocities in this direction after breakup, as quantified later.

Given that results available thus far concerning the breakup regimes of liquid jets in crossflow are relatively independent of Ohnesorge number Oh and q, values of Weber number We for the various breakup regime transitions are summarized in Table 2 for the results of Mazallon et al.[1] and the present investigation. Values of Weber number We at the breakup regime transitions for the two studies are in excellent agreement for the column/bag and multimode/shear breakup regime transitions. There are greater differences between the two studies for the bag/multimode breakup regime transition, but this is not surprising due to problems of quantitatively defining the appearance of this transition. Notably, similar difficulties have been encountered when this transition was identified for the secondary breakup of drops subjected to shock wave disturbances.[20] Finally, the breakup regime transitions for the secondary breakup of drops due to shock wave disturbances are also

Table 2 Summary of breakup transitions of round liquid jets in gaseous crossflows[a]

Source	Mazallon et al.[1,b]	Present investigation[c]
Column/bag breakup transition	5	4
Bag/multimode breakup transition	60	30
Multimode/shear breakup transition	110	110

[a]For round nonturbulent liquid jets in gaseous crossflows.
[b]Test conditions: $\rho_L/\rho_G = 700$–1100, $We = 0$–200, $q = 100$–8000, and $Oh < 0.3$.
[c]Test conditions: $\rho_L/\rho_G = 683$–1033, $We = 0.5$–260, $q = 3$–450, and $Oh < 0.29$.

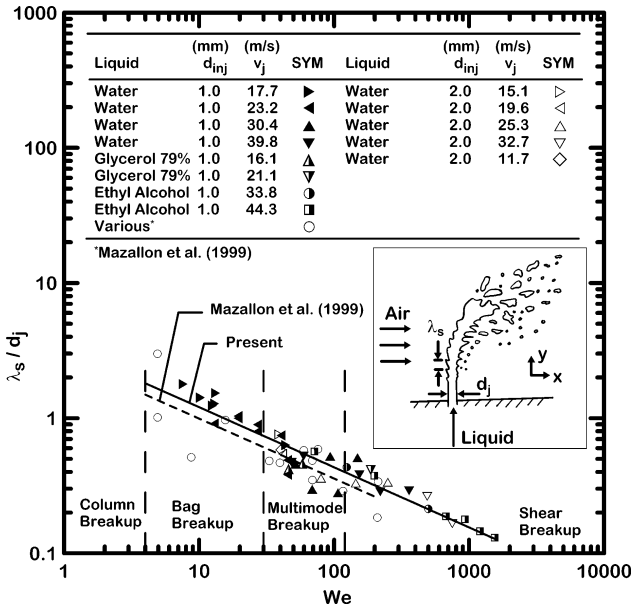

Fig. 3 Liquid surface wavelengths as a function of Weber number for nonturbulent round liquid jets in gaseous crossflow.

plotted in Fig. 2, based on the measurements of Hsiang and Faeth[20]; these findings are in surprisingly good agreement with the results for primary breakup of nonturbulent round liquid jets in crossflow (aside from the absence of a bag-breakup/liquid-column-breakup transition, for which there is no counterpart for the secondary breakup of drops), suggesting a similarity of the general features of these two liquid breakup processes.

Liquid Surface Waves

Insight concerning the mechanisms of primary breakup of round nonturbulent liquid jets in crossflow can be gained by considering the properties of waves that appear along the surface of the liquid jet during the breakup process. Examples of these waves can be seen in Fig. 1 for all flows involving breakup. The wavelength λ_s of these disturbances along the liquid surface was taken to be the distance between nodes for liquid column breakup; in contrast, they were best observed on the upstream side of the liquid jet for the bag, multimode, and shear breakup regimes, as shown in the inset of Fig. 3. The wavelength results illustrated in Fig. 3 include the measurements of Mazallon et al.[1] and the present investigation. The experimental uncertainties (95% confidence) of the wavelengths shown in Fig. 3 are estimated to be smaller than 25%, largely due to wavelength irregularities similar to those seen in Fig. 1. Finally, the breakup regime transitions, found as discussed in connection with Figs. 1 and 2 and Table 2, are also shown for reference.

The wavelength measurements of Mazallon et al.[1] and the present investigation shown in Fig. 3 agree within experimental uncertainties. Both results indicate that the values of λ_s/d_j lead quite naturally to the breakup regimes shown in Fig. 1, recalling the tendency of λ_s/d_j to progressively decrease with increasing Weber number of the crossflow, as follows: Column breakup involves $\lambda_s/d_j > 1$,

which is consistent with the tendency of this breakup mode to involve stretching of the entire liquid column between nodes, with final breakup first involving the strained liquid column between the nodes as well; bag breakup involves $\lambda_s/d_j \approx 1$, which is consistent with the somewhat axisymmetric deflection of the flow to form a bag; shear breakup insvolves $\lambda_s/d_j \approx 0.1$, which is consistent with the formation of ligament structures having a diameter similar to λ_s around the periphery of the jet that eventually separate from the downstream side of the liquid jet to form drops; and finally with the multimode region being associated with values of λ_s/d_j of 0.1–1.0, which is consistent with the complex geometry of this region, ranging from behavior in the bag breakup regime to the shear breakup regime.

The formation of the waves that are present on the upstream side of the liquid jet involves flow in the vicinity of its upstream stagnation point. In this region, the main effect of the crossflow is to tend to accelerate the lesser density gaseous crossflow toward the greater density liquid jet in the cross stream direction. Such conditions provide a classical prescription for the development of Rayleigh/Taylor instabilities. The best-fit correlation of the wavelength measurements was achieved as a function of Weber number alone, as shown in Fig. 3. For values of $Oh < 0.12$ and values of q in the range 3–8000, this correlation can be expressed as follows:

$$\lambda_s/d_p = 3.4We^{-0.45}, \qquad We > 4 \tag{1}$$

where the correlation coefficient of the fit is 0.82.

Liquid Surface Velocities

Before turning to consideration of liquid breakup properties, the environment of the breakup process will be defined by considering mean streamwise liquid surface properties for round nonturbulent liquid jets in gaseous crossflow. This information was obtained by measuring the streamwise velocity of small disturbances on the surface of the liquid jet, using double-pulse shadowgraphs. The measurements were designed so that experimental uncertainties of these measurements (95% confidence) at a given condition along the liquid surface were less than 10%, similar to the other results reported in this investigation.

Present measurements of mean streamwise liquid surface velocities, normalized by the mean jet exit velocity at each condition, are plotted as a function of normalized streamwise distance from the jet exit, y/y_b, in Fig. 4. It was possible to obtain reliable measurement of v_s/v_j in the range $y/y_b = 0.1$–0.7. Observable disturbances on the liquid surface were rare for $y/y_b < 0.1$, whereas the surface becomes difficult to define near the liquid jet breakup condition $y/y_b > 0.7$, which accounts for the limited range of the measurements in Fig. 4. The results in Fig. 4, however, suggest that $v_s/v_j = 1$ within experimental uncertainties. This provides further evidence of the relatively weak interaction between the streamwise motion of the liquid jet and the gaseous crossflow that has already been seen in the breakup visualization of Fig. 1, in Fig. 1a, when no gaseous crossflow was present.

Onset of Breakup

A feature of the primary breakup of round nonturbulent liquid jets in gaseous crossflow is that there is relative universality of liquid column deformation at the onset of breakup for some of the breakup regimes, similar to the secondary breakup of drops subject to shock wave disturbances. In particular, Mazallon et al.[1] observed the deformation of round nonturbulent liquid jets in crossflow using two laser beams separated by a 45-deg angle to obtain two simultaneous shadowgraphs. These observations showed that the cross-sectional area of liquid jets during this type of deformation was preserved so that the cross stream dimension increased as the streamwise dimension decreased. Given this background, present observations of deformation were simplified by only considering measurements of the streamwise jet dimensions. These observations are shown in Fig. 5, where the ratio of the initial jet diameter to the minimum streamwise dimension of the liquid jet at the onset of drop formation, d_j/d_i, is plotted as a function of Weber number, with $We > 4$. These conditions involve breakup in the bag, multimode, and shear breakup regimes. Measurements shown in Fig. 5 include results from Mazallon et al.[1] and the present investigation for primary breakup of round nonturbulent liquid jets in crossflow, along with the results of Hsiang and Faeth[20] for the secondary breakup of drops subjected to shock wave disturbances. The various primary breakup regime boundaries for round nonturbulent liquid jets in crossflow, for example, bag, multimode, and shear breakup, are also shown for reference. For bag breakup, $d_j/d_i \approx 2$ independent of Weber number, which is in excellent agreement with the results for the onset of secondary breakup of drops subjected to shock wave disturbances for all breakup regimes and values of Weber number studied (see Refs. 18–20). In contrast to behavior for the secondary breakup of drops, however, values of d_j/d_i for breakup of round nonturbulent liquid jets in crossflow decrease in the multimode primary breakup regime before reaching a constant value once again with $d_j/d_i \approx 1$ in the shear breakup regime. This difference in behavior was

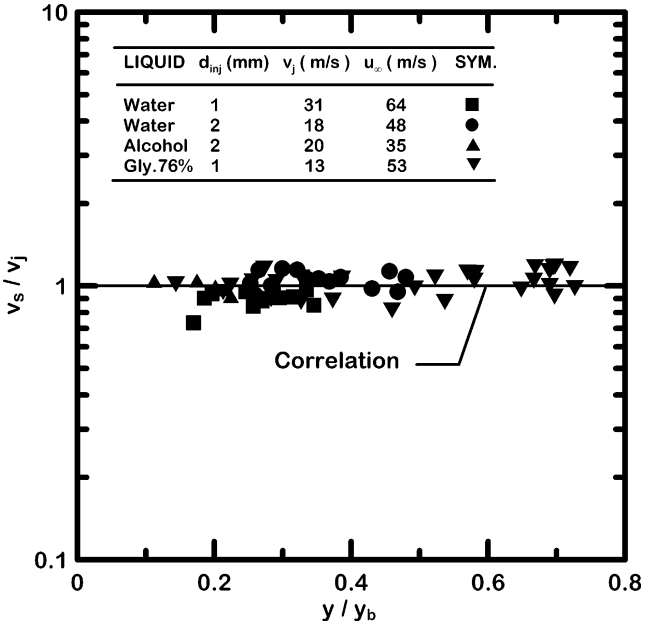

Fig. 4 Mean liquid surface velocities in streamwise direction as a function of streamwise distance from jet exit.

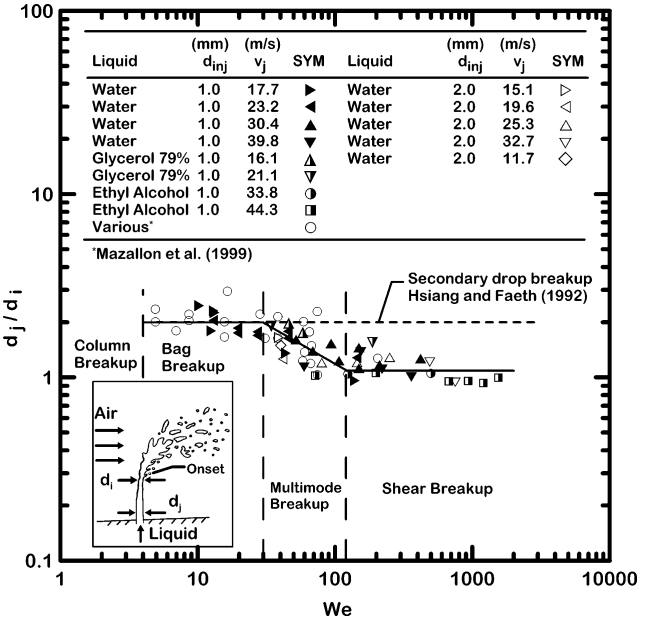

Fig. 5 Deformation at onset of primary breakup as a function of Weber number for nonturbulent round liquid jets in gaseous crossflow.

observed for the full range of q and Ohnesorge number considered during the present investigation. The reason for these differences of deformation properties between the onset of drop formation for primary breakup of round nonturbulent liquid jets in crossflow and the secondary breakup of drops, however, is not known.

Additional consideration of the onset of breakup was limited to the shear breakup regime. Within this regime, the appearance of drops was always preceded by the appearance of ligaments protruding downstream from the region near the sides of the liquid jet toward the wake behind the jet due to the crossflow. Analogous to earlier findings for the onset of ligament and drop formation during the turbulent primary breakup of round turbulent liquid jets in still gases due to Sallam and Faeth,[27] ligament diameters at the onset of ligament formation were found by equating the momentum flux (relative to bulk liquid in the jet) of a ligament of given size, $d_{\ell i}$, to the maximum surface tension force required to start the formation of a ligament of this size. Treatment of the momentum of the present nonturbulent liquid, however, had to be modified from its treatment for a turbulent liquid by Sallam and Faeth.[27] In the present case, it was assumed that liquid motion required to form a ligament originated from the viscous shear layer beginning at the upstream stagnation point of the crossflow and growing at the periphery of the liquid jet due to the motion of the gaseous crossflow before separating from the liquid jet on the downstream side of the crossflow. Then the characteristic liquid phase velocity of this shear layer, due to viscous effects, is

$$u_L \sim u_\infty \Big/ [1 + (\mu_L \rho_L / (\mu_G \rho_G))^{\frac{1}{2}}] \tag{2}$$

When the momentum of the liquid shear layer near the surface is equated to the surface tension force required by the hemispherical distortion of the liquid surface that must be overcome to form a ligament having a diameter $d_{\ell i}$, there results

$$\rho_L u_L^2 d_{\ell i}^2 \sim \sigma d_{\ell i} \tag{3}$$

When u_L^2 in Eq. (3) is substituted from Eq. (2) and it is noted that $\rho_G/\rho_L \ll \mu_L/\mu_G$, there results

$$d_{\ell i}/d_j = C_{\ell i}(\mu_L/\mu_G)/We \tag{4}$$

where $C_{\ell i}$ is an empirical constant associated with the onset of ligament formation on the order of unity. Finally, when Rayleigh breakup of the drops at the end of the ligaments is assumed, which appeared to be the most common mechanism of drop formation based on visualization of the present flows, there results

$$d_{pi}/d_{\ell i} = C_{pi} \tag{5}$$

where C_{pi} is an empirical constant associated with the onset of drop formation on the order of unity.

Present measurements of the ligament diameter at the onset of ligament formation, $d_{\ell i}$, and the present mean drop diameter at the onset of drop formation, d_{pi}, are plotted as a function of $(\mu_L/\mu_G)/We$, as suggested in Eqs. (4) and (5), in Fig. 6. Within a finite diameter liquid jet, the shear layer along the periphery of the jet from which the ligaments form cannot grow indefinitely; therefore, there are two branches of ligament diameter behavior:

$$d_{\ell i}/d_j = 0.07[(\mu_L/\mu_G)/We]^{\frac{1}{2}}, \qquad (\mu_L/\mu_G)/We < 2.0 \tag{6}$$

$$d_{\ell i}/d_j = 0.095, \qquad (\mu_L/\mu_G)/We > 2.0 \tag{7}$$

The standard deviations of the power and coefficient in Eq. (6) are 18 and 6%, respectively, whereas the standard deviation of the constant on the right-hand side of Eq. (7) is 24%. The reduction of the power in Eq. (6) from 1 to $\frac{1}{2}$ in Eq. (6) is statistically significant. This discrepancy appears to be due to the limitations that the finite diameter of the liquid layer places on the growth of the shear layer, when it is noted that the shear layer is eventually limited to a fixed fraction of the liquid jet diameter at conditions where this power

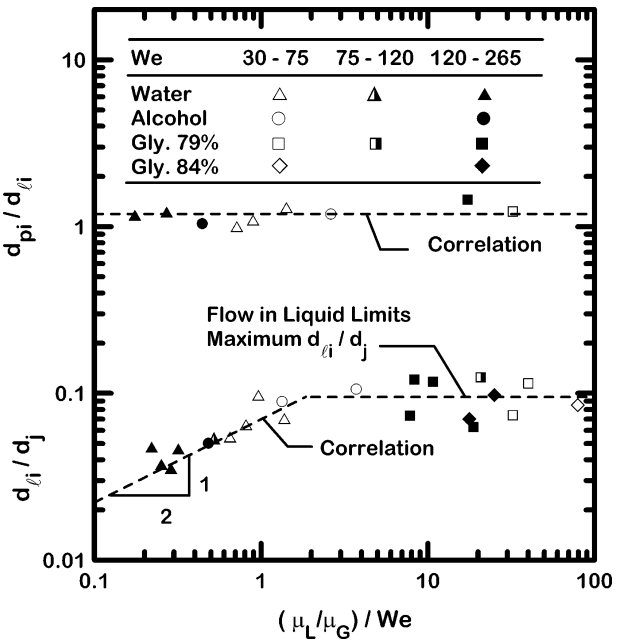

Fig. 6 Ligament and drop sizes at onset of primary breakup for nonturbulent round liquid jets in gaseous crossflow.

must become zero. Finally, Rayleigh breakup implies a constant ratio of the drop and ligament diameters:

$$d_{pi}/d_{\ell i} = 1.2 \tag{8}$$

where the standard deviation of the constant on the right-hand side of Eq. (8) is 0.14.

The next property of the onset of ligament formation that was considered was the distance along the liquid jet, $y_{\ell i}$, where this occurs. First, motion along the liquid jet is simply given as a function of time by the liquid jet convection velocity, based on present observations, for example,

$$y_{\ell i} = v_j t_{\ell i} \tag{9}$$

then the diameter of the ligament at onset should be proportional to the thickness of the liquid shear layer, which is assumed to grow according to the well-known viscous shear layer growth rate expression $(\nu_L t)^{1/2}$. This implies that

$$d_{\ell i} \sim (\nu_L t_{\ell i})^{\frac{1}{2}} \tag{10}$$

Substituting for $d_{\ell i}$ from Eq. (6) and rearranging then yields

$$t_{\ell i} \Big/ t_v^* = C_t(\mu_L/\mu_G)/We \tag{11}$$

where

$$t_v^* = d_j^2 \Big/ \nu_L \tag{12}$$

and C_t is an empirical constant associated with the onset of ligament formation on the order of unity.

Values of $t_{\ell i}$ were found from present measurements of $y_{\ell i}$ using Eq. (9). These measurements are plotted as a function of $(\mu_L/\mu_G)/We$, as suggested by Eq. (11), in Fig. 7. It is evident that the measurements correlate quite well according to the relationship of Eq. (11) as

$$t_{\ell i} \Big/ t_v^* = 0.0004[(\mu_L/\mu_G)/We] \tag{13}$$

where the standard deviations of the power of the parameter in brackets and coefficient in Eq. (13) are 2.5 and 0.6%, respectively. The coefficient of Eq. (13) seems small, but this parameter actually is $C_t C_{\ell i}^2$ and is small because $C_{\ell i}$ is small from Eq. (6), whereas $C_t \approx 0.3$, which is on the order of unity, as expected.

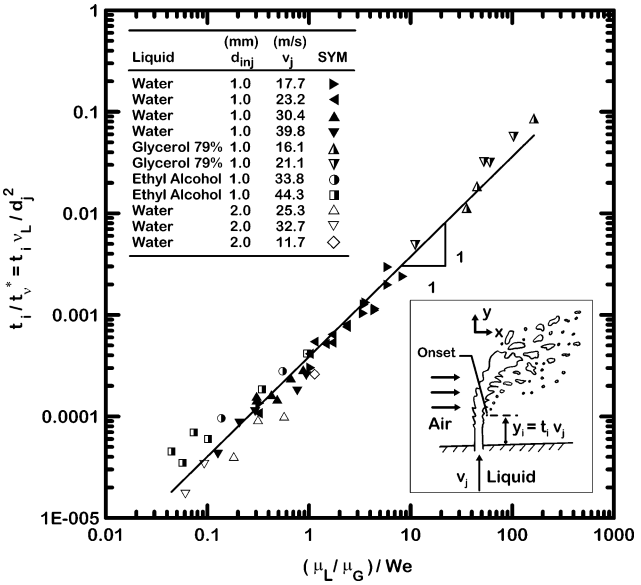

Fig. 7 Time of onset of ligament formation for nonturbulent round liquid jets in gaseous crossflow.

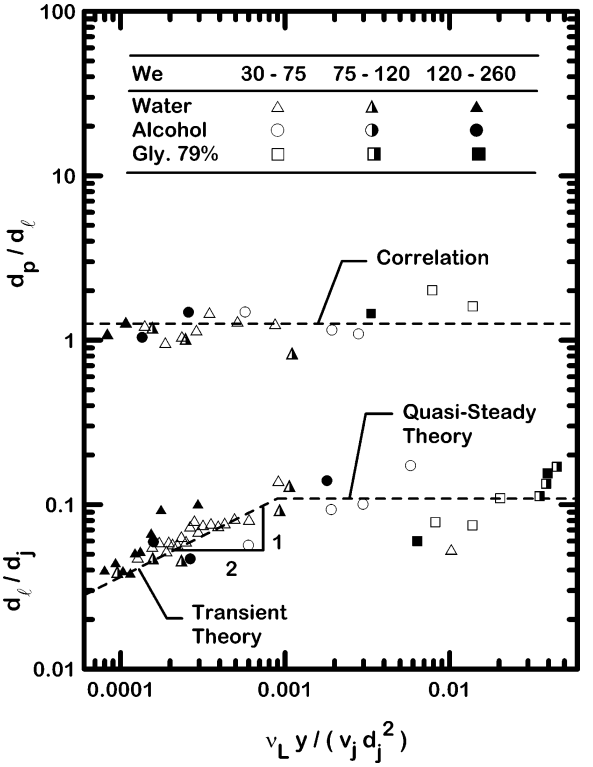

Fig. 8 Diameters of ligaments and drops for primary breakup as function of distance along jet for nonturbulent round liquid jets in gaseous crossflow.

Ligament and Drop Sizes Along the Liquid Surface

To consider ligament and drop sizes along the liquid surface, times required to reach specific distances along the liquid surface were found from the convection approximation of Eq. (9). A second limitation was to consider ligament and drop formation only in the shear breakup regime as opposed to the more complex bag and multimode breakup regimes; fortunately, shear breakup tends to dominate practical applications. Finally, velocities associated with the formation of ligaments were assumed to be from the shear layer as given by the shear layer approximation of Eq. (2). Then, similar to observations concerning the onset of ligament formation, the variation of ligament size along the surface was assumed to involve a transient regime where the thickness of the shear layer is growing as a function of time as

$$\delta(t)/d_j \sim \left(v_L t \big/ d_j^2\right)^{\frac{1}{2}} = \left(t \big/ t_v^*\right)^{\frac{1}{2}} \tag{14}$$

and a quasi-steady regime where the shear becomes a fixed fraction of the liquid jet diameter, which in turn is taken to be proportional to the initial liquid jet diameter or

$$\delta/d_j = C_\ell \tag{15}$$

where C_ℓ is an empirical constant associated with the shear layer thickness having a magnitude on the order of 0.1 similar to the similar parameter found for the onset of ligament formation from Eq. (7). As before, assuming that $d_\ell \sim \delta$, and fitting the results to the present measurements, finally yields, for the transient regime,

$$d_\ell/d_j = 3.6\left[v_L y \big/ \left(v_j d_j^2\right)\right]^{\frac{1}{2}}, \qquad v_L y \big/ v_j d_j^2 < 0.001 \tag{16}$$

and for the quasi-steady regime,

$$d_\ell/d_j = 0.11, \qquad v_L y \big/ \left(v_j d_j^2\right) > 0.001 \tag{17}$$

where the standard deviations of the power and coefficient in Eq. (16) are 13 and 98%, respectively, and the standard deviation of the constant in Eq. (17) is 0.04. Finally, the relationship between ligament and drop diameters along the liquid surface proved to be identical to this relationship at onset conditions, as expected, or from Eq. (8),

$$d_p/d_\ell = 1.2 \tag{18}$$

with the standard deviation of this constant of 0.27, as before. In addition, the result given in Eq. (18) is appropriate for both the transient and quasi-steady regimes of liquid surface breakup. Present measurements of the variation of ligament and drop sizes along the liquid surface are plotted according to Eqs. (16–18) in Fig. 8; these results are very similar to the onset results of Fig. 6, and Figs. 6 and 8 are also consistent with each other through the time of onset of ligament formation of Fig. 7. Finally, these results also support the hypothesis that drop formation occurs by the mechanism of Rayleigh breakup at the tips of ligaments.

Drop Velocity Properties

Drop velocities after breakup were measured using double-pulse shadowgraphy in regions where the dispersed flow region was dilute and using double-pulse holography in regions where the dispersed flow region was dense. These measurements were obtained close to the tips of ligaments to minimize effects of drop velocity relaxation to the ambient velocity. The resulting drop velocity distributions along the initial direction of the jet, v_p, and along the initial direction of the crossflow, u_p, are shown in Fig. 9. It is evident that both components of drop velocity are nearly independent of the drop diameter. An apparent exception to this behavior involves small drops with d_p/SMD < 0.5, where SMD denotes Sauter mean diameter; however, this behavior is felt to be an artifact of the relatively fast relaxation times of small drops compared to large drops. The velocity normalizations used in Fig. 9 were chosen to compare v_p with the initial jet velocity v_j and u_p with the characteristic liquid velocity component in the cross stream direction given by Eq. (2). The resulting velocity correlations of the measurements in Fig. 9 are as follows:

$$v_p/v_j = 0.7 \tag{19}$$

$$u_p/u_L = u_p(\rho_L/\rho_G)^{\frac{1}{2}} \big/ u_\infty = 6.7 \tag{20}$$

where the uncertainties (95% confidence) of the constants on the right-hand sides of Eqs. (19) and (20) are comparable to the uncertainties (95% confidence) of the measurements themselves, or 10%. Measurements of both velocity components indicate some effects of gas-phase drag during the breakup process on the velocities of drops after breakup. These effects tend to reduce the v_p component from

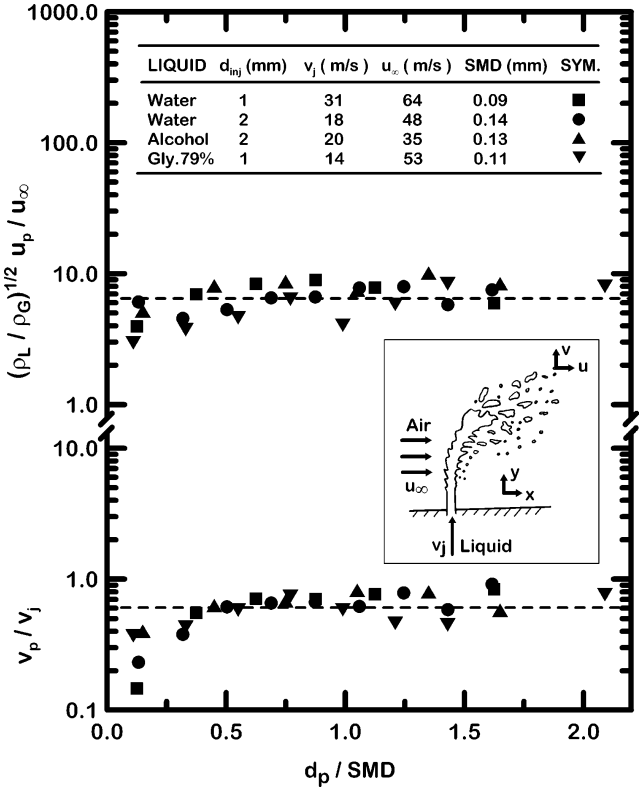

Fig. 9 Streamwise and crosstream drop velocity distributions after primary breakup of nonturbulent round liquid jets in gaseous crossflow.

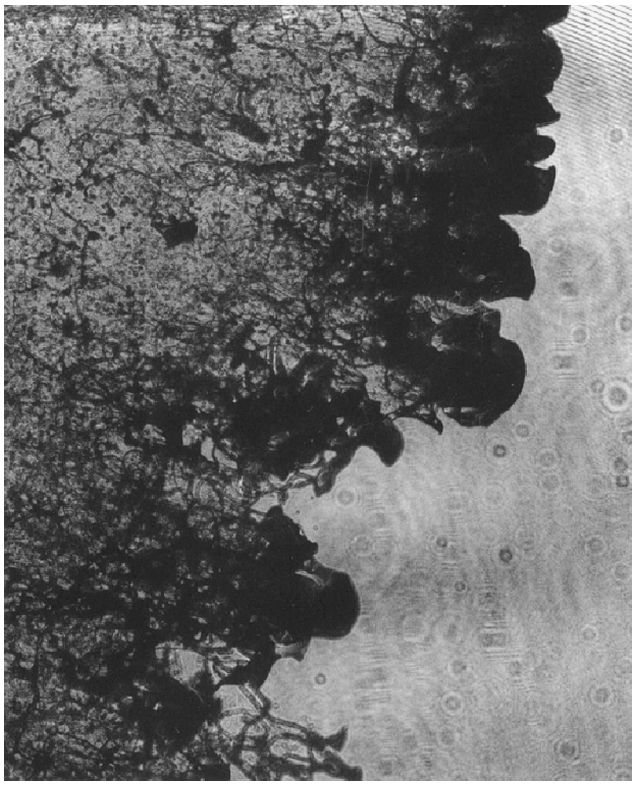

Fig. 10 Pulsed shadowgraph of the end of the liquid core for nonturbulent round liquid jets in gaseous crossflow within shear breakup regime: glycerol 79%, $d_j = 0.9$ mm, $u_\infty = 73$ m/s, $v_j = 38$ m/s, $We = 132$, and $q = 218$.

v_j to some extent and to increase the u_p component significantly from u_L.

Liquid Column Breakup

Figure 10 is a typical pulsed shadowgraph of the end of the liquid core for nonturbulent liquid jets in gaseous crossflow, within the shear breakup regime. It can be seen that the jet appears to disintegrate into droplike segments that subsequently undergo secondary drop breakup. Similar to other measurements during this investigation, sufficient observations of this length were made to achieve an average liquid column breakup length within the experimental uncertainties mentioned earlier.

The locations of the completion of the primary breakup process for the bag, multimode, and shear breakup regimes were analyzed similar to the earlier treatment of nonturbulent liquid columns in crossflow due to Wu et al.[2] and turbulent liquid column breakup lengths due to Sallam et al.[24] This was done by associating the time of penetration of liquid elements in the jet with the time of secondary breakup of drops due to shock wave disturbances. When this approach is adopted, the time required for bag, multimode, and shear breakup is given by an expression analogous to that used for the secondary drop breakup times due to shock wave disturbances from Hsiang and Faeth[20]:

$$t_b / t^* = C_{yb} \tag{21}$$

where t^* is the characteristic liquid-phase time of Ranger and Nicholls,[28]

$$t^* = (\rho_L/\rho_G)^{\frac{1}{2}} d_j / u_\infty \tag{22}$$

and C_{yb} is an empirical constant associated with the time of breakup of the liquid column on the order of unity. Finally, consideration of cross stream momentum yields the following simple result that was first observed by Wu et al.,[2]

$$x_b/d_j = C_{xb} \tag{23}$$

where C_{xb} is an empirical constant associated with the cross stream penetration of the liquid column on the order of unity.

Measurements of t_b and x_b from the present investigation are plotted according to Eqs. (21) and (23) in Fig. 11 as a function of Weber number for small Ohnesorge number conditions. The Weber number for breakup regime transitions at small Ohnesorge number are also shown for reference. As noted earlier, present results are limited to the bag, multimode, and shear breakup regimes, where drop formation occurs along the liquid surface as is generally desired for practical atomization purposes. As anticipated from earlier measurements of drop breakup times for the secondary breakup of drops exposed to shock wave disturbances, the ratio t_b/t^* is relatively independent of Weber number for the three breakup regimes, yielding $C_{yb} = 2.5$ with an experimental uncertainty (95% confidence) of 7%. This is comparable but somewhat smaller than $C_{yb} = 6.0$ for the secondary breakup of drops from Dai and Faeth.[23] These differences are not surprising due to the fundamental differences of liquid breakup for a round liquid jet in crossflow and a spherical drop subjected to a shock wave disturbance. Finally, measurements of x_b/d_j from both Wu et al.[2] and the present investigation yield the surprisingly simple result, $C_{xb} = 8.0$, with an experimental uncertainty (95% confidence) of 9%.

Nonturbulent round liquid jets in crossflow undergo a different mechanism of liquid column breakup as a whole, namely, as classical Rayleigh breakup, than the other breakup regimes. In this case, the length of the liquid column at the time of breakup can be correlated based on Weber's[29] observations that the breakup length L_b of a round nonturbulent viscous liquid jet can be expressed as follows:

$$L_b/d_j \sim \left(\rho_L d_j v_j^2 / \sigma\right)^{\frac{1}{2}} + 3\mu_L v_j/\sigma \tag{24}$$

Then with application of the convection approximation of Eq. (9), the following expression for the time of breakup, t_b, of the liquid column as a whole in the liquid column breakup regime is obtained,

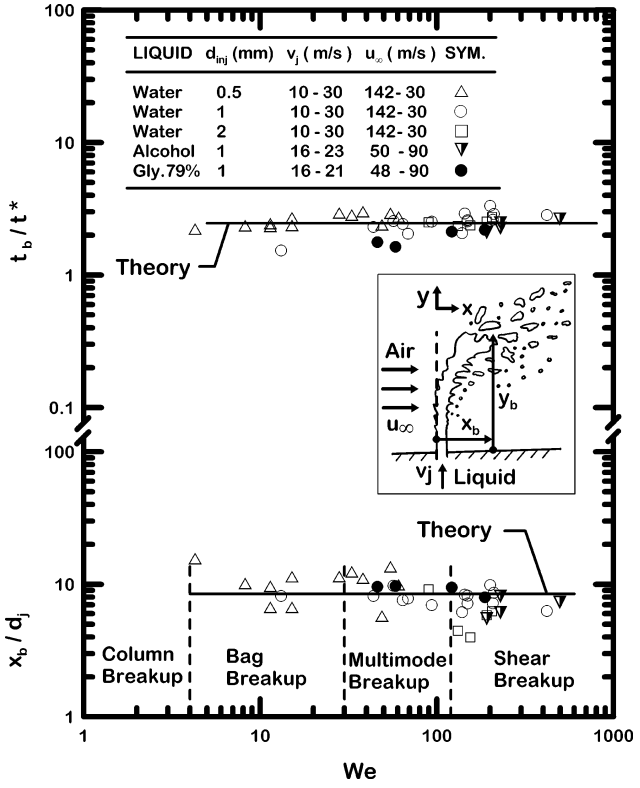

Fig. 11 Location of end of liquid jet in the streamwise and crosstream directions during primary breakup of nonturbulent round liquid jets in gaseous crossflow in bag, multimode, and shear breakup regimes.

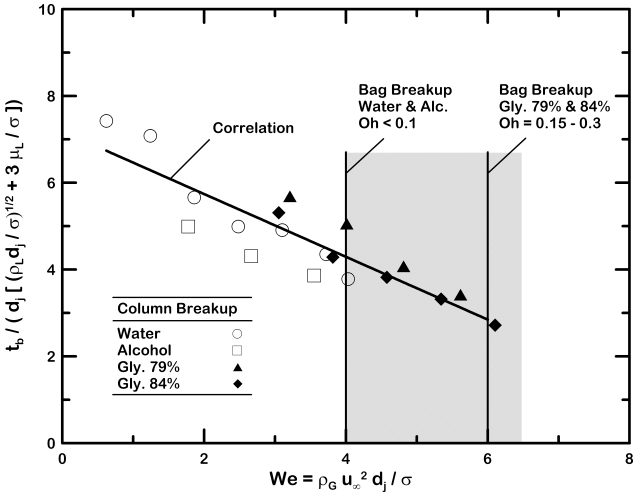

Fig. 12 Time of breakup of the liquid column for nonturbulent round liquid jets in gaseous crossflow in liquid column breakup regime.

as follows:

$$t_b \Big/ \left\{ d_j \left[(\rho_L d_j/\sigma)^{\frac{1}{2}} + 3\mu_L/\sigma \right] \right\} \sim \text{const} \tag{25}$$

Present measurements of liquid column breakup times, normalized according to Eq. (25), are plotted as a function of Weber number in Fig. 12. The results show that subjecting a liquid column to increasing crossflow velocities progressively reduces the time that it takes for the liquid column to break up into droplets. As the Weber number approaches the critical value near the onset of bag breakup, the liquid column breakup times display a smooth transition to the time for the onset of bag breakup in Fig. 10. For Weber numbers close to zero, on the other hand, the present results approach the measurements of Sterling and Sleicher[30] for breakup lengths of various liquids ejecting from short injectors ($L/d \cong 0.25$) into still air at comparable jet exit velocities.

The correlation of the liquid column breakup time results in Fig. 12 is remarkable, the present range of test liquids with liquid viscosities spanning two orders of magnitude is considered. This indicates that, even under the influence of crossflow, the breakup of nonturbulent liquid columns can be related to the Rayleigh breakup mechanism right up to the onset of bag breakup. These results also emphasize the importance of considering the viscous terms in Eq. (24) for liquids having large viscosities. (See additional discussion of this point in Wu et al.[31]) Finally, the correlation of the present measurements of liquid column breakup times in Fig. 12 is as follows:

$$t_b \Big/ \left\{ d_j \left[(\rho_L d_j/\sigma)^{\frac{1}{2}} + 3\mu_L/\sigma \right] \right\} = 7.20 - 0.73We$$
$$0.5 \le We \le 6 \tag{26}$$

where the standard deviation of the power and coefficient in Eq. (26) are 0.34 and 0.09, respectively.

Liquid Breakup Rates Due to Nonturbulent Primary Breakup

The next liquid surface property that was studied during the present investigation was the flux of liquid drops relative to the liquid surface due to nonturbulent primary breakup along the liquid surface. This was done for the shear breakup regime (Fig. 1) in a manner somewhat different from earlier studies of this property for turbulent primary breakup of plane and round liquid jets in still gases due to Sallam and Faeth.[27] In particular, for the shear breakup regime in crossflow, the drops formed by primary breakup only leave the liquid column over its downstream half (Fig. 1), as opposed to the entire periphery of a turbulent liquid jet in still gases. Thus, in the present case, liquid drops due to primary breakup only leave the liquid column over the downstream projected area of the liquid column, with the drops having a relative velocity u_p with respect to the liquid column. Thus, averaging the liquid removal rate over this downstream projected area to find the average mass flux of liquid drops leaving the liquid column, $\dot{m}''_f$, a liquid surface breakup efficiency factor ε is defined as

$$\varepsilon = \dot{m}''_f/(\rho_f u_p) \tag{27}$$

where the limit $\varepsilon = 1$ represents conditions where liquid drops form in a continuous manner over all of the downstream projected area of the liquid. The actual appearance of liquid surface during nonturbulent primary shear breakup, particularly as the result of Rayleigh breakup at the tips of growing ligaments along the surface, however, suggests that ε is usually less than unity. Naturally, it is expected that ε approaches zero near the onset of drop formation due to nonturbulent primary breakup.

Present measurements of ε for primary breakup of nonturbulent round liquid jets in gaseous crossflow in air at normal temperature and pressure are shown in Fig. 13. The independent variable used is the dimensionless streamwise length y/y_b between the jet exit and the condition where the liquid jet breaks up as a whole. The limit giving the onset of nonturbulent primary breakup along the liquid surface for present test conditions is also in Fig. 13. This limit does not correlate in the same manner as ε and appears as a band rather than a line in Fig. 13 as a result. Typical of earlier measurements of ε due to Sallam and Faeth[27] for round turbulent jets in still environments, ε is on the order of 10^{-3} at the onset of primary breakup and crudely approaches unity as the condition for breakup of the liquid jet as a whole is approached. The best-fit correlation of present measurements of ε for nonturbulent round liquid jets in gaseous crossflow, which is shown in Fig. 13, is as follows:

$$\varepsilon = 6.89E-04 \exp(5.43 y/y_b) \tag{28}$$

The standard deviations of the exponential and preexponential factors appearing on the right-hand side of Eq. (28) are 19 and 13%, respectively, and the correlation coefficient of the fit is 0.90, which is reasonably good. Moreover, the trends of the measurements appearing in Fig. 13 are reasonable with small values of ε near the onset

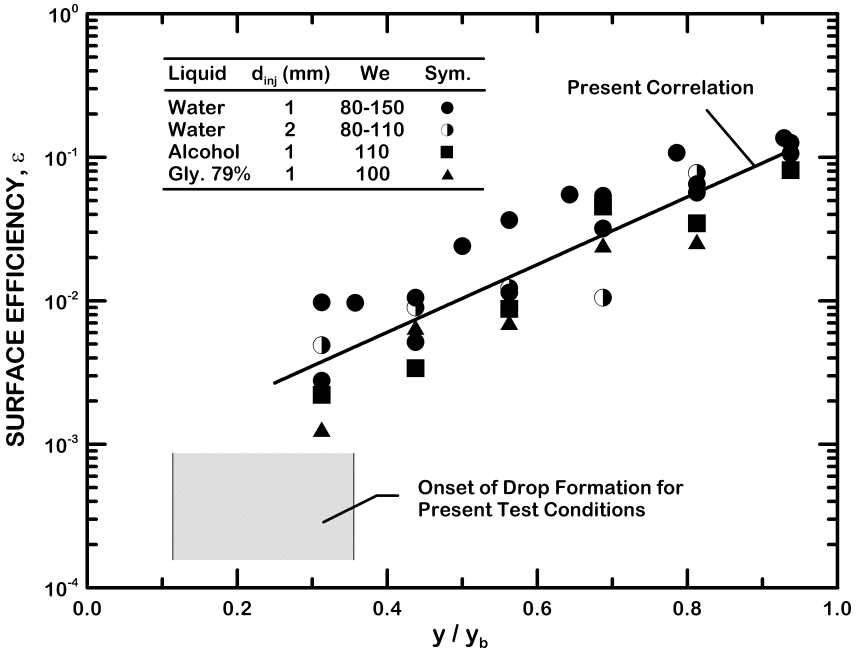

Fig. 13 Mean surface efficiency factors as function of streamwise distance along liquid column between onset of drop formation and location of the end of liquid jet.

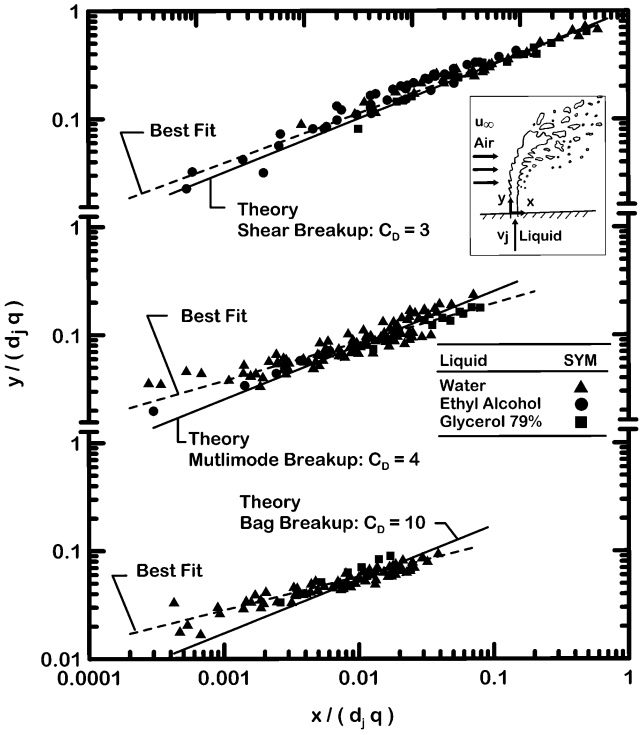

Fig. 14 Liquid column trajectories in the streamwise and crosstream directions during primary breakup of nonturbulent round liquid jets in gaseous crossflow.

of breakup approaching values of ε having an order of magnitude of unity as the end of the liquid column is approached.

Liquid Column Trajectories

The liquid jet trajectory was considered next because drops formed at the surface of the liquid jet naturally eminate from locations along the jet in the x, y plane. In this case, simplified analysis following Wu et al.[2] was used, considering flow in the bag, multimode, and shear breakup regimes. The analysis was based on convection at the jet exit velocity in the jet streamwise direction. The results for the cross stream direction were based on conservation of momentum, assuming a constant drag coefficient based on the jet exit diameter for each breakup regime. The evaluation of the predictions using present measurements is in Fig. 14. The measurements and predictions have been grouped according to the breakup regime, yielding best-fit values of the measurements of $C_D = 3$, 4, and 10 for the shear, multimode, and bag breakup regimes, respectively. Recall that the drag coefficients in the cross stream analysis are based on the jet exit diameter; this variation of C_D is expected as a natural way to account for the deformation of the liquid jets in the various breakup regimes as discussed in connection with Fig. 5.

Conclusions

The formation of ligaments and drops along the liquid jet surface, as well as the deformation, deflection, and extent of the liquid jet itself, were studied experimentally for round nonturbulent liquid jets in air crossflow at normal temperature and pressure. Test conditions included water, ethyl alcohol, and glycerol (79 and 84%) jets injected normal to the crossflow for the following ranges of test variables (when combined with the earlier study of Mazallon et al.[1]): crossflow Weber numbers of 0–2000, liquid/gas momentum ratios of $q = 3$–8000, liquid/gas density ratios of $\rho_L/\rho_G = 683$–1033, and Ohnesorge numbers of $Oh = 0.003$–0.29. The major conclusions of the study were as follows:

1) There is a useful general analogy between the primary breakup of round nonturbulent liquid jets in crossflow and the secondary breakup of drops subjected to shock wave disturbances, which suggests modest streamwise interactions in the liquid jets, for example, liquid breakup properties were not strongly affected by the liquid/gas momentum ratio for values smaller than 8000, which was the largest value considered during the present and earlier investigations.

2) Transitions between the various breakup regimes are not influenced significantly by liquid viscosities for $Oh < 0.3$ and by liquid jet exit velocities for $q < 8000$. Transitions to bag, multimode, and shear breakup occurred at $We = 4$, 30, and 110, which were in reasonably good agreement with earlier results for round nonturbulent liquid jets in crossflow from Mazallon et al.[1] These results were also in qualitative agreement with earlier results for the secondary breakup of drops due to shock wave disturbances from Hsiang and Faeth.[20]

3) There were two regimes for both the onset of ligament formation along the liquid surface and for the variation of ligament diameter as a function of distance along the liquid surface: first, an initial transient regime associated with the growth of a shear layer near the liquid surface that which supplies liquid to the base of ligaments and, second, a quasi-steady regime, where the shear layer reaches its maximum possible growth within the confines of the round liquid jet and has a thickness that is a fixed fraction of the liquid jet diameter.

4) In both regimes of ligament growth, drops formed at the tips of ligaments were a fixed multiple of the ligament diameter; thus, this behavior generally supports drop formation at the tips of ligaments by the classical Rayleigh breakup mechanism.

5) Drop velocity distributions after breakup were relatively independent of drop size and approximated the liquid jet velocity v_j in the y direction but were somewhat larger than the characteristic liquid-phase velocity in the x direction, u_L, due to drag on the drops by the cross flowing gas as the drops are formed.

6) Breakup of the liquid column as a whole in the bag, multimode, and shear breakup regimes approximated the total times of breakup of drops subjected to shock wave disturbances in the bag, multimode, and shear breakup regimes, yielding $t_b/t^* = 2.5$ and $x_b/d_j = 8.0$, with the latter result in good agreement with the earlier measurements of Wu et al.[2] In contrast, liquid column breakup as a whole in the liquid column breakup regime was better represented by Rayleigh breakup of a viscous round nonturbulent liquid jet as proposed by Weber.[29]

7) The mean drop mass flux over the downstream projected area of the liquid column, $\dot{m}''_f$, due to nonturbulent primary breakup at the liquid surface could be correlated by the dimensionless length along the liquid column, y/y_b. Quite plausibly, ε was small near the onset of drop formation due to nonturbulent primary breakup but reached values on the order of unity as the end of the liquid column of the jet is approached.

Acknowledgments

This research was sponsored by the Air Force Office of Scientific Research, Grants, F49620-99-1-0083 and F49620-02-1-0007, under the technical management of J. M. Tishkoff. The assistance of R. Jolly and D. Ma under the Undergraduate Research Opportunity Program of the University of Michigan is gratefully acknowledged. The U.S. Government is authorized to make copies of this paper for governmental purposes notwithstanding any copyright notation thereon.

References

[1]Mazallon, J., Dai, Z., and Faeth, G. M., "Primary Breakup of Nonturbulent Round Liquid Jets in Gas Crossflows," *Atomization and Sprays*, Vol. 9, No. 3, 1999, pp. 291–311.

[2]Wu, P.-K., Kirkendall, K. A., Fuller, R. P., and Nejad, A. S., "Breakup Processes of Liquid Jets in Subsonic Crossflows," *Journal of Propulsion and Power*, Vol. 13, No. 1, 1997, pp. 64–73.

[3]Geary, E. L., and Margettes, M. J., "Penetration of a High Velocity Gas Stream by a Water Jet," *Journal of Spacecraft and Rockets*, Vol. 6, No. 1, 1969, pp. 79–81.

[4]Reichenbach, P. R., and Horn, K. P., "Investigation of Injectant Properties in Jet Penetration in a Supersonic Stream," *AIAA Journal*, Vol. 9, No. 3, 1971, pp. 469–471.

[5]Kush, E. A., and Schetz, J. A., "Liquid Jet Injection into a Supersonic Flow," *AIAA Journal*, Vol. 11, No. 9, 1979, pp. 1223, 1224.

[6]Schetz, J. A., and Paddye, A., "Penetration of a Liquid Jet in Subsonic Airstreams," *AIAA Journal*, Vol. 15, No. 10, 1977, pp. 1385–1390.

[7]Schetz, J. A., Kush, E. A., and Joshi, P. B., "Wave Phenomena in Liquid Jet Breakup in a Supersonic Crossflow," *AIAA Journal*, Vol. 15, No. 6, 1979, pp. 774–778.

[8]Nejad, A. S., and Schetz, J. A., "Effects of Properties and Locations in the Plume or Droplet Diameter for Injection in a Supersonic Stream," *AIAA Journal*, Vol. 21, No. 7, 1983, pp. 956–961.

[9]Nejad, A. S., and Schetz, J. A., "Effects of Viscosity and Surface Tension on a Jet Plume in Supersonic Crossflow," *AIAA Journal*, Vol. 22, No. 4, 1984, pp. 458, 459.

[10]Less, D. M., and Schetz, J. A., "Transient Behavior of Liquid Jets Injected Normal to a High-Velocity Gas Stream," *AIAA Journal*, Vol. 24, No. 12, 1986, pp. 1979–1985.

[11]Kitamura, Y., and Takahashi, T., "Stability of a Liquid Jet in Air Flow Normal to the Jet Axis," *Journal of Chemical Engineering of Japan*, Vol. 9, No. 4, 1976, pp. 282–286.

[12]Nguyen, T. T., and Karagozian, A. R., "Liquid Fuel Jet in a Subsonic Crossflow," *Journal of Propulsion Power*, Vol. 8, No. 1, 1992, pp. 21–29.

[13]Karagozian, A. R., "Analytical Model for the Vorticity Associated with a Transverse Jet," *AIAA Journal*, Vol. 24, No. 3, 1986, pp. 429–436.

[14]Higuera, F. J., and Martinez, M., "An Incompressible Jet in a Weak Crossflow," *Journal of Fluid Mechanics*, Vol. 249, 1993, pp. 73–97.

[15]Wu, P.-K., Miranda, R. F., and Faeth, G. M., "Effects of Initial Flow Conditions on Primary Breakup of Nonturbulent and Turbulent Round Liquid Jets," *Atomization and Sprays*, Vol. 5, No. 2, 1995, pp. 175–196.

[16]Lienhard, J. H., "Velocity Coefficients for Free Jets from Sharp-Edged Orifices," *Journal of Fluids Engineering*, Vol. 106, No. 1, 1984, pp. 13–17.

[17]Schlichting, H., *Boundary Layer Theory*, 4th ed., McGraw-Hill, New York, 1960, pp. 72, 73.

[18]Hsiang, L.-P., and Faeth, G. M., "Near-Limit Drop Deformation and Secondary Breakup," *International Journal of Multiphase Flow*, Vol. 18, No. 5, 1992, pp. 635–652.

[19]Hsiang, L.-P., and Faeth, G. M., "Drop Properties After Secondary Breakup," *International Journal of Multiphase Flow*, Vol. 19, No. 5, 1993, pp. 721–735.

[20]Hsiang, L.-P., and Faeth, G. M., "Drop Deformation and Breakup Due to Shock Wave and Steady Disturbances," *International Journal of Multiphase Flow*, Vol. 21, No. 4, 1995, pp. 545–560.

[21]Chou, W.-H., Hsiang, L.-P., and Faeth, G. M., "Temporal Properties of Drop Breakup in the Shear Breakup Regime," *International Journal of Multiphase Flow*, Vol. 23, No. 4, 1997, pp. 657–669.

[22]Chou, W.-H., and Faeth, G. M., "Temporal Properties of Secondary Drop Breakup in the Bag Breakup Regime," *International Journal of Multiphase Flow*, Vol. 24, No. 6, 1998, pp. 889–912.

[23]Dai, Z., and Faeth, G. M., "Temporal Properties of Secondary Breakup in the Multimode Breakup Regime," *International Journal of Multiphase Flow*, Vol. 27, No. 2, 2001, pp. 217–236.

[24]Sallam, K. A., Dai, Z., and Faeth, G. M., "Drop Formation at the Surface of Plane Turbulent Liquid Jets in Still Gases," *International Journal of Multiphase Flow*, Vol. 25, No. 6-7, 1999, pp. 1161–1180.

[25]Lange, N. A., *Handbook of Chemistry*, 8th ed., Handbook Publishers, Sandusky, OH, 1984, pp. 13–17.

[26]Hinze, J. O., "Fundamentals of the Hydrodynamic Mechanism of Splitting in Dispersion Processes," *AIChE Journal*, Vol. 1, No. 3, 1955, pp. 289–295.

[27]Sallam, K. A., and Faeth, G. M., "Surface Properties During Primary Breakup of Turbulent Liquid Jets in Still Air," *AIAA Journal*, Vol. 41, No. 8, 2003, pp. 1514–1524.

[28]Ranger, A. A., and Nicholls, J. A., "The Aerodynamic Shattering of Liquid Drops," *AIAA Journal*, Vol. 7, No. 2, 1969, pp. 285–290.

[29]Weber, C., "Zum Zerfall eines Flussigkeitsstrahles," *Zeitschreif Angewesen. Mathematik und Mechanik*, Vol. 2, 1931, pp. 136–141.

[30]Sterling, A. M., and Sleicher, C. A., "The Instability of Capillary Jets," *Journal of Fluid Mechanics*, Vol. 63, Pt. 3, 1975, pp. 477–495.

[31]Wu, P.-K., Tseng, L.-K., and Faeth, G. M., "Primary Breakup in Gas/Liquid Mixing Layers for Turbulent Liquids," *Atomization and Sprays*, Vol. 2, No. 3, 1992, pp. 295–317.

S. Aggarwal
Associate Editor